RECENT DEVELOPMENTS IN COMPUTATIONAL AND APPLIED MECHANICS
B.D. Reddy (Ed.)

EFFICIENT COMPUTATIONAL ASPECTS FOR ANALYSIS OF SHEET STAMPING PROBLEMS

G.A. Duffett[1], P. Cendoya[1], J. Rojek[2] and E. Oñate[1]

[1] *International Center for Numerical Methods in Engineering (CIMNE)*
Edificio C1, Campus Norte UPC
Gran Capitán s/n, 08034 Barcelona
Spain

[2] *Institute of Fundamental Technological Research*
Swietokrzyska 21
00-049 Warsaw
Poland

Abstract

Efficiency and accuracy are vital for the acceptable simulation of large scale industrial sheet stamping problems. Two aspects, implemented within the explicit dynamic program STAMPACK, that effectively address this problem are described: an anisotropic plasticity material model combined with a thin shell element that contains only displacement degrees of freedom and an effective drawbead formulation based on an elastic-plastic analogy.

1 Introduction

The simulation of large scale industrial sheet stamping problems requires the combination of many numerical methods in order to achieve an acceptable result. Industrial problems tend to be geometrically complex and the large deformation, large strain, material plasticity, friction and contact properties of the problem must be considered for even the simplest simulations. Due to the complexity of the analysis and the strain rates involved the use of explicit dynamic technology has many advantages.

Explicit dynamic programs are more efficient and contain simpler algorithms than their implicit counterparts but the analyses require an enormous number of time steps, due in part to the conditional stability of the methods. This aspect places further emphasis on the efficiency of the methodologies utilised in these applications

[1]The authors wish to acknowledge the support of other members of the software development and support team, Jose Duarte who kindly donated the experimental picture of the S-rail, and the European Community for their support grants.

and many researchers have turned their attention towards this aspect since efficiency without loss of accuracy is all-important. It should be noted that parallel processing techniques fall outside the range of this paper; this will be documented in other publications (Duffett *et al* (1997)) but it is noted that any efficiency gained from new algorithms will generally aid parallel versions of the software.

The work described in this paper addresses two new developments where efficiency and accuracy are vital for the acceptable simulation of sheet stamping processes. A generalised anisotropic plasticity material model has been included within a newly developed shell element containing only displacement degrees of freedom (Oñate and Zarate (1996), Cendoya (1996)). This couples a highly effective element for explicit dynamic analyses with an efficient coding strategy to obtain accurate results for simulations of this type.

The action of drawbeads is vital to the behaviour of the sheet during stamping operations but the curvatures of these drawbeads are often very large compared to the curvatures of the other tools and dies. This requires a very fine descretization of the sheet mesh which, not only increases the mesh size, but reduces the critical time step that may be utilised with the resulting increase in computational cost. The approach used here is to implement an effective drawbead based on an elasto-plastic analogy to compute the drawbead restraining force as a function of the relative displacement of the sheet across the drawbead line.

The effectiveness of these techniques is shown by means of examples obtained from the most recent NUMISHEET conferences (Makinouchi *et al* (1993), Lee *et al* (1996)).

2 Numerical Methodology

2.1 Explicit dynamic formulation

The dynamic equilibrium equations are written in terms of the principle of virtual work using an updated Lagrangian formulation. The discretized form of equilibrium is obtained in the standard manner (Zienkiewicz and Taylor (1991)):

$$\mathbf{M}\ddot{\mathbf{r}}^t + \mathbf{C}\dot{\mathbf{r}}^t = \mathbf{R}^t - \mathbf{F}^t - \mathbf{F}_c^t \qquad (1)$$

where M is the mass matrix, C the damping matrix, $\ddot{\mathbf{r}}$ the vector of nodal accelerations, $\dot{\mathbf{r}}$ the vector of nodal velocities, R the vector of external loading, F the vector of internal forces and $\mathbf{F}_c$ the vector of contact forces, all evaluated at time t.

A diagonal mass matrix obtained by a lumping procedure applied to the element consistent mass matrices is used and the damping matrix is assumed to be proportional to this via $\mathbf{C} = 2\alpha\mathbf{M}$, α being a damping parameter. The equations of motion are integrated by the central difference method and, using the assumption that the M and C matrices are diagonal, this gives rise to the explicit dynamic formulation which allows the configuration at time $t + \Delta t$ to be computed from the known deformed configuration at time t.

Conditional stability of the explicit time integration requires that the time step size must not exceed a critical time step size related to the lowest period of vibration $\Delta t_{crit} < \frac{2}{\omega}$. Using an approximation to the critical time step size for each element $\Delta t^{(e)}_{crit}$ allows a critical time step size to be computed at each step (or at pre-determined intervals) which therefore provides an automatic time-stepping procedure.

2.2 Contact and Friction

Contact plays a vital role in sheet stamping since the sheet is in contact with all the tools (punch, blankholder and dies). This contact is treated by using a standard penalty formulation with friction conditions governed by a Coulomb model. To improve the efficiency of solution selective node to segment and node to patch search strategies have been implemented (Wriggers (1995)).

3 Anisotropic elasto-plastic material model

A general elasto-plastic material model is considered where the elastic behaviour is assumed to be isotropic and an anisotropic plane stress model based on Hill's theory (Hill (1979)) is assumed for the plastic part. The particular expression of the yield function used is (Dodd and Caddell (1984))

$$|\sigma_1 + \sigma_2|^M + (1 + 2R)|\sigma_1 - \sigma_2|^M = 2(1 + R)\sigma_y^M \tag{2}$$

where the Lankford coefficient is given by

$$R = (R_0 + 2R_{45} + R_{90})/4\,. \tag{3}$$

From equation (2) the standard quadratic yield function of Hill's is recovered for $M = 2$ and the isotropic von Mises yield function is obtained for $R = 1$ and $M = 2$.

This material is highly desirable for sheet stamping operations but it is computationally expensive. In the current implementation an efficient coding strategy is used but its power is based on the implementation within a thin shell element that itself is highly efficient.

3.1 Basic Shell Triangle (BST) Element

The BST shell element developed is suitable for the analysis of shells allowing for large displacements and large strains. The shell deformation is described in terms of the deformation of its midsurface which is decomposed into the membrane and bending states. Thus, with the assumption of the Kirchhoff hypothesis, the rate of deformation tensor at any point of the shell $\dot{\mathbf{e}} = \{\dot{e}_{xx}\,,\ \dot{e}_{yy}\,,\ \dot{e}_{xy}\}^{\mathrm{T}}$ can be written as

$$\dot{\mathbf{e}} = \dot{\boldsymbol{\varepsilon}} + z\dot{\boldsymbol{\kappa}} \tag{4}$$

where $\dot{\boldsymbol{\varepsilon}} = \{\dot{\varepsilon}_{xx}\,,\ \dot{\varepsilon}_{yy}\,,\ \dot{\varepsilon}_{xy}\}^{\mathrm{T}}$ is the rate of membrane deformation of the midsurface, $\dot{\boldsymbol{\kappa}} = \{\dot{\kappa}_{xx}\,,\ \dot{\kappa}_{yy}\,,\ \dot{\kappa}_{xy}\}^{\mathrm{T}}$ is the rate of bending deformation of the midsurface with z being the normal distance of the material point from the shell midsurface. The effectiveness of this element arises from the fact that $\dot{\boldsymbol{\kappa}}$ is written only in terms of displacement degrees of freedom related to a patch of elements as shown in Figure 1.

Using standard finite element interpolation the rate of membrane deformation can be related to the element nodal velocities $\dot{\mathbf{x}}^{(e)} = \{\dot{\mathbf{x}}_1^{(e)}\,,\ \dot{\mathbf{x}}_2^{(e)}\,,\ \dot{\mathbf{x}}_3^{(e)}\}^{\mathrm{T}}$ via

$$\dot{\boldsymbol{\varepsilon}} = \mathbf{B}_{\mathrm{m}}\,\dot{\mathbf{x}}^{(e)}\,, \tag{5}$$

where $\mathbf{B}_{\mathrm{m}}$ is an operator matrix. Linear interpolation of the element nodal velocities $\dot{\mathbf{x}}^{(e)}$ leads to a constant rate of membrane deformation tensor within an element; the operator matrix $\mathbf{B}_{\mathrm{m}}$ is then equivalent to the standard plane stress Constant Strain Triangle element (Zienkiewicz and Taylor (1991)).

The approach developed by Oñate and Cervera (1993) enables the constant element curvature to be written in terms of the edge rotations which are, in turn, written in terms of the displacements of the nodes belonging to the patch of elements

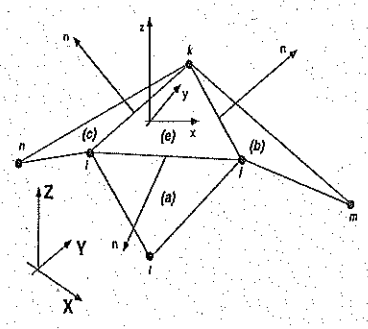

Figure 1: Element patch surrounding a shell element (e) with vertices ijk

surrounding the element under consideration. This implies

$$\dot{\kappa} = \mathbf{B}_\mathrm{b}\, \dot{\mathbf{a}}^{(e)}, \tag{6}$$

where $\mathbf{B}_\mathrm{b}$ is the operator matrix and $\dot{\mathbf{a}}^{(e)} = \{\dot{\mathbf{x}}^{(e)}, \dot{\mathbf{x}}^{(a)}, \dot{\mathbf{x}}^{(b)}, \dot{\mathbf{x}}^{(c)}\}^\mathrm{T}$ is the vector of nodal velocities of a certain patch of elements (a),(b) and (c) surrounding the (e)-th element as seen in Figure 1.

Combining relations (5) and (6) in equation (4) enables the rate of deformation tensor at any point of the shell $\dot{\mathbf{e}}$ to be expressed in terms of nodal translational velocities only. More details and the explicit form of the matrices $\mathbf{B}_\mathrm{m}$ and $\mathbf{B}_\mathrm{b}$ can be found in Oñate and Zarate (1996) and Cendoya (1996).

The element stresses are computed in the local element system at each time increment using the condition of plane stress. Objectivity is preserved and the use of small time increments in explicit dynamic analysis allows the use of

$$^{t+\Delta t}\boldsymbol{\sigma} = {}^{t}\boldsymbol{\sigma} + \mathbf{D}\Delta e^{n+1/2} \tag{7}$$

noting that the stresses ${}^{t}\boldsymbol{\sigma}$ must be rotated to the $t+\Delta t$ configuration before the sum (7) is performed. Constant volume of the element in the plastic range is preserved by updating the element thickness at each time increment.

4 Drawbead Methodology

Drawbeads are used in sheet stamping in order to restrain the sheet between the blankholder and the dies. This restricts the movement of the sheet in the drawing

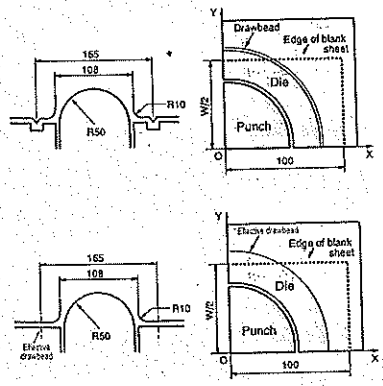

Figure 2: Geometry of stamping tools showing real and effective drawbeads

direction and, since the final result is greatly altered, this needs to be accurately modelled. However, drawbead curvatures tend to be very large compared to the curvatures of the other tools, and this requires a very fine descretization of the sheet thereby increasing the computational cost (note that the sheet passes through the drawbead).

To overcome these problems an effective drawbead formulation has been implemented making use of an elasto-plastic analogy to compute the drawbead force. This formulation replaces the geometrical representation of the drawbead with a line fixed on the tool surface and passing through the drawbead centres as shown in Figure 2.

This restraining force f_drawb which acts tangential to the sheet and normal to the drawbead line is a function of the amount of drawing u_draw, defined as the relative displacement of the sheet with respect to the drawbead in the direction normal to the drawbead line. Therefore we have

$$f_\mathrm{drawb} = \begin{cases} C^\mathrm{el}_\mathrm{drawb} u_\mathrm{draw} & \text{if } |C^\mathrm{el}_\mathrm{drawb} u_\mathrm{draw}| \le f^\mathrm{max}_\mathrm{drawb} \\ f^\mathrm{max}_\mathrm{drawb} \dfrac{C^\mathrm{el}_\mathrm{drawb} u_\mathrm{draw}}{|C^\mathrm{el}_\mathrm{drawb} u_\mathrm{draw}|} & \text{if } |C^\mathrm{el}_\mathrm{drawb} u_\mathrm{draw}| > f^\mathrm{max}_\mathrm{drawb} \end{cases} \tag{8}$$

where $C^\mathrm{el}_\mathrm{drawb}$ is called the *elastic modulus of the drawbead* and $f^\mathrm{max}_\mathrm{drawb}$ is the maximum force the drawbead can sustain. These characteristic parameters have been referred to the unit length, so the total restraining force acting on the drawbead segment needs to be integrated over the length l_drawb. The function in equation (8) for the drawbead force is analogous to an elasto-plastic material model and hence similar

procedures may be used to compute this force.

However, before the correct forces can be determined, the intersection of the sheet elements with the drawbead line must be found. Simpler forms of the search algorithms used for the contact algorithms are used for this and the incremental drawing can be determined for each element on the drawbead line. The plastic return algorithm can then be used to compute the drawbead force and distribute it to the segment nodes of the sheet elements, thereby restraining the motion of the sheet.

4.1 Elasto-plastic analogy

The computation of the drawbead restraining force can be carried out using the following elasto-plastic analogy. The drawing velocity v_{draw} is decomposed into a reversible ("elastic") part $v^{\text{rv}}_{\text{draw}}$ and an irreversible ("plastic") part $v^{\text{ir}}_{\text{draw}}$

$$v_{\text{draw}} = v^{\text{rv}}_{\text{draw}} + v^{\text{ir}}_{\text{draw}} \tag{9}$$

allowing the constitutive equation for a drawbead to be written as

$$\dot{f}_{\text{drawb}} = C^{\text{el}}_{\text{drawb}}(v_{\text{draw}} - v^{\text{ir}}_{\text{draw}}) \tag{10}$$

where $\dot{f}_{\text{drawb}}$ is an objective rate of the restraining force. The irreversible relative "flow" is governed by the following rule

$$v^{\text{ir}}_{\text{draw}} = \lambda \frac{\partial \Phi}{\partial f_{\text{drawb}}} \quad , \quad \Phi = f^2_{\text{drawb}} - (f^{\max}_{\text{drawb}})^2 \tag{11}$$

where Φ is a drawbead "yield condition" and the parameter λ obeys the classical Kuhn–Tucker complementary conditions $\lambda \geq 0$, $\Phi \leq 0$, $\lambda\Phi = 0$, summarizing the possible loading/unloading situations and the consistency requirement $\lambda\dot{\Phi} = 0$ if $\Phi = 0$.

5 Numerical Examples

The formulations described have been implemented within the STAMPACK software code (Stampack User Manual (1996)) developed by the authors and to illustrate their potential two examples from recent NUMISHEET conferences have been examined.

5.1 Deep drawing of a square cup

This example reproduces one of the benchmark tests of NUMISHEET'93 (Makinouchi *et al.* (1993)). This is a deep drawing simulation of a square cup where drawbeads have been added to the original test allowing numerical comparisons to be made with the work of Kawka *et al.* (1994).

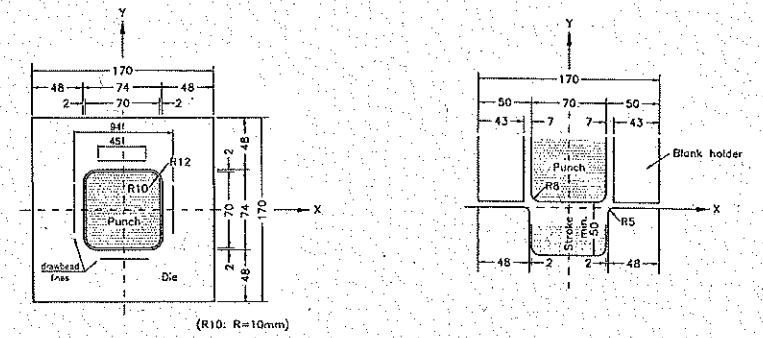

Figure 3: Geometrical definition of the square cup deep drawing problem

The geometrical description of the test including the drawbeads is shown in Figure 3. Because of symmetry only one quarter of the cup was analyzed using a regular mesh for the sheet of 1800 BST elements and the anisotropic material model with hardening. Problem details can be obtained in the NUMISHEET'93 reference, but the effective drawbead parameters are given as: "elastic modulus" of the drawbead $C^{\text{el}}_{\text{drawb}} = 21.7$ N/mm^2, maximum drawbead force $f^{\max}_{\text{drawb}} = 82.5$ N/mm.

Comparison of the thickness strain when no drawbeads are present is given in Figure 4 where an average of the experimental results presented at NUMISHEET'93 is also shown. Figure 5 shows the fully deformed shape of the sheet after the drawing process. These results show favourable agreement with others presented.

With drawbeads present the behaviour of the sheet alters somewhat. In Figure 6 a comparison of the final sheet outline with and without drawbeads shows that the sheet draws in less with the drawbeads (shown as straight lines in the figure). The anticipated evolution of the restraining force in the drawbeads considered is shown in Figure 7 where the elasto-plastic anology can be clearly seen. The value of the fully developed drawbead force obtained in the simulation is 1856 N and is in perfect agreement with the expected value of 1856.25 N predicted analytically.

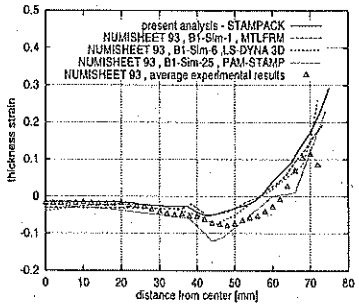

Figure 4: Thickness strain comparisons along line from centre of sheet to the corner

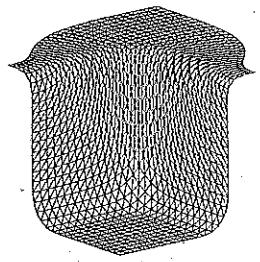

Figure 5: The deformed shape for the fully drawn square cup

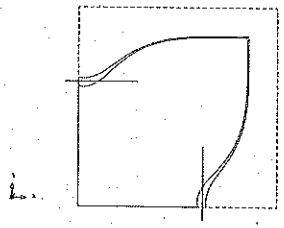

Figure 6: Comparison of sheet outline with and without drawbeads

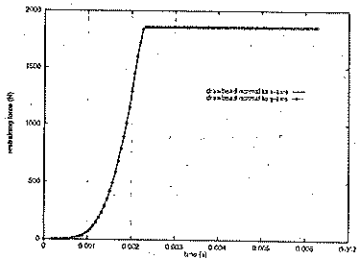

Figure 7: Evolution of the restaining forces in the drawbeads

These results compare very well with the NUMISHEET'93 results (no drawbeads) as well as with those presented by Kawka *et al* (1994) where drawbeads were considered. The increase of CPU when the drawbeads were included was practically insignificant, so the efficiency and accuracy goals of the algorithm were both achieved.

5.2 Deep drawing of a S-rail

The second example considered is the deep drawing of a steel S-rail defined in the NUMISHEET'96 conference (Lee *et al* (1996)). This problem simulates the stamping and elastic springback of the rail (wrinkling and springback cause many manufacturing problems).

The geometry of the rail, the problem description and the problem details can be found in the NUMISHEET'96 reference. The complete sheet was modelled with a mesh of 12000 BST elements using Hill's plasticity model; the complete mesh for sheet and tools is shown in Figure 8 (note that the stamping direction is upwards).

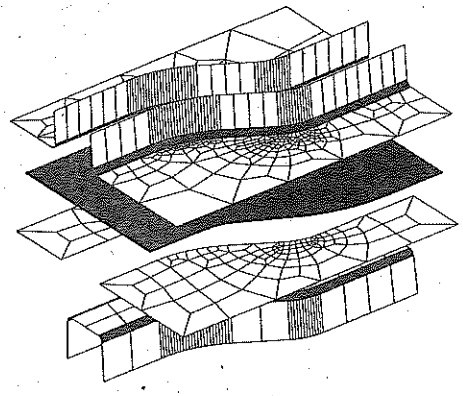

Figure 8: Initial setup for S-rail benchmark problem showing, from top to bottom, the die, sheet (fine mesh), blankholders and punch

The analysis was run in two stages: (1) stamping, where the results agree very favourably with those presented in NUMISHEET'96 (see Cendoya (1996)) and (2) springback, where the tools were removed and the rail was allowed to recover. The final deformed shape after the springback stage is shown in Figure 9. The buckling of the surfaces is clearly seen and a comparison with experimental results, given in Figure 10, indicates the good agreement that was obtained. Various cross-sections of the rail were also compared with excellent agreement.

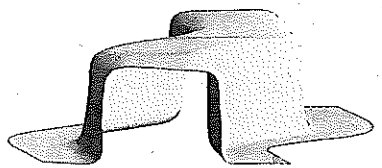

Figure 9: Deformed shape after springback (front view)

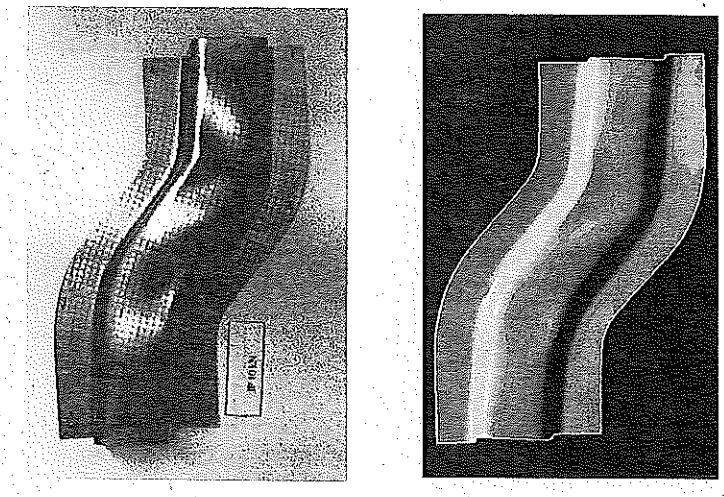

Figure 10: Final deformed shapes obtained by experiment and simulation

The results presented here show good agreement with the numerical and experimental results presented at NUMISHEET'96. This problem contains both bending and drawing zones and therefore validates the effectiveness of the current methodologies.

6 Conclusions

This paper presented two highly successful aspects for improving the efficiency while maintaining the accuracy of sheet stamping analyses based on the explicit dynamic methodology:

(1) a generalised anisotropic material model has been implemented within the Basic Shell Triangle (BST) element which incorporates bending and membrane effects and requires only translational displacements as the final nodal variables. The computational cost of this element is marginally higher than that for a membrane formulation.

(2) an effective drawbead formulation based on an elasto-plastic analogy has proved to be very simple to utilise, accurate and incurs only minimal additional computational cost.

These aspects have both been proved via examples to be simple, efficient and accurate. They are therefore excellent for use in explicit dynamic programs for the simulation of large scale industrial sheet stamping problems.

References

Cendoya, P. (1996) Non-linear explicit analysis of shells using a shell triangle with translational degrees of freedom, (in Spanish), *Ph.D. Thesis*, Universidad Politécnica de Cataluña, Barcelona.

Dodd, B. and Caddell, R. (1984) On the anomalous behaviour of anisotropic sheet metals, *Int. J. Mech. Sci.* **26**, n. 2, 113–118.

Duffett, G.A., Oñate, E., Rojek, J. and Zarate, F. (1997) Stampar: A Parallel Processing Approach to Sheet Stamping Simulations. Computational Plasticity, eds. Owen, D.R.J., Oñate, E. and Hinton, E. CIMNE, Barcelona.

Hill, R. (1979) Theoretical Plasticity of Textured Aggregates, *Math. Proc. Camb. Phil. Soc.* **85**, 179.

Lee, J.K., Kinsel, G.L. and Wagoner, R.H. (eds.) (1996) NUMISHEET'96 Numerical Simulation of 3D Sheet Metal Forming Processes - Verification of Simulations with Experiments, Dearborn, Michigan, USA.

Makinouchi, A., Nakamachi, E., Oñate, E. and Wagner, R. (eds.) (1993) Proceedings of the International Conference NUMISHEET'93, Riken, Tokyo.

Oñate, E. and Cervera, M., (1993) Derivation of thin plate bending elements with one degree of freedom per node: a simple three node triangle, *Engng. Comput.* **10**, 543–61.

Oñate, E. and Zarate, F., (1996) Shell triangles with translational degrees of freedom, *Research Report*, CIMNE, Barcelona.

STAMPACK User Manual (1996) An explicit dynamic finite element package for sheet stamping anlaysis. CIMNE, Barcelona.

Wriggers, P. (1995) Finite element algorithms for contact problems, *Arch. of Comp. Meth. in Engng.* **2**, n. 4, 1–51.

Zienkiewicz, O.C. and Taylor, R.L. (1991) The finite element method, 4th Edition, Mc-GrawHill, Vol. I, 1990, Vol. II, 1991.